Hybrid model for the prediction of residual stresses induced by 15-5PH steel turning

Alexandre Mondelin, Frédéric Valiorgue, Joël Rech, Michel Coret, Éric Feulvarch

Hybrid model for the prediction of residual stresses induced by 15-5PH steel turning

Alexandre Mondelin [a,b], Frédéric Valiorgue [a,*], Joël Rech [a], Michel Coret [b], Eric Feulvarch [a]

[a] Université de Lyon, ENISE, LTDS, UMR CNRS 5513, 58 Rue Jean Parot, 42023 Saint-Etienne, France
[b] Université de Lyon, INSA, LaMCoS, UMR CNRS 5259, 27 Avenue Jean Capelle, 69621 Villeurbanne, France

This study presents the development of a hybrid model for the prediction of residual stresses induced during the finish turning of a 15-5PH martensitic stainless steel. This new approach consists in replacing tool and chip modeling by equivalent loadings. This model is called "hybrid" because it applies thermomechanical loadings (obtained experimentally) on a numerical model. These equivalent loadings are moved onto the machined surface to compute the final residual stress state.

The first part of the present research work proposed to characterize machining equivalent thermo-mechanical loadings at the machined surface level. A new simple method is presented. The case of the dry orthogonal cutting operation of a 15-5PH martensitic stainless steel with coated carbide tools is treated. To this end, two experimental devices and associated numerical models are used. Shapes and locations of equivalent thermo-mechanical loadings are extracted from a Finite Element (FE) simulation of orthogonal cutting. A simplified analytical approach is applied to draw up a list of parameters necessary to calibrate the equivalent loadings. These parameters (friction coefficient, contact length, cutting forces etc.) have to be quantified experimentally. So, tribological tests and orthogonal cutting tests are performed. Finally, using experimental results, machining equivalent thermo-mechanical loadings are quantified. The heat flux, tangential stress and normal pressure at the final workpiece surface are characterized as a function of the cutting speed and the feed.

In the second part of this paper, machining equivalent thermo-mechanical loadings previously identified are transferred to a 3D configuration. The objective is to predict the residual stresses induced by a longitudinal finish turning operation on 15-5PH steel.

Based on this new approach, the paper also aims at investigating the interactions between each revolution. It is shown that around five revolutions are necessary to reach a steady state for this material. Finally the numerical results are compared with experimental measurements obtained by X-Ray diffraction. It is shown that residual stresses cannot be considered as homogeneous over the surface due to the feed influence. Additionally, the X-Ray beam is too large to quantify this heterogeneity. Based on average numerical values coherent with the average values obtained by X-Ray diffraction, it is shown that the numerical model provides consistent results compared to experimental measurements for a large feed range.

Keywords:
Friction
Hybrid model
Residual stresses
Turning
X-ray diffraction

1. Introduction

Precipitated hardening (PH) stainless steels (like a 15-5PH steel) show excellent mechanical properties, low distortion, excellent weldability and good corrosion resistance. That is why they are used in aerospace and nuclear industries. Moreover, predicting the fatigue resistance of mechanical parts is crucial for these industries. Several studies [1,2] have shown that fatigue resistance is directly and significantly influenced by several parameters such as surface roughness, residual stress and microstructure, which are commonly summarized by the term "surface integrity" [3]. The influence of surface integrity on the functional performance and life of machined components has been widely discussed in the literature [4]. For example, Yang et al. [5] and Liu and Yang [6] have reported the significant role that residual stresses play in determining the fatigue life of critical product. Regarding the residual stresses, there is a general consensus that near surface compressive stresses are beneficial for the lifespan (depending on the depth and magnitude of the compressive stress) [7], and can negate/counter the impact of some surface imperfections (roughness). Conversely, high tensile residual stresses at the surface leads to a much shorter fatigue life [8].

* Corresponding author.
E-mail addresses: alexandre.mondelin@enise.fr (A. Mondelin), alexandre.mondelin@enise.fr (F. Valiorgue).

Nomenclature

V_c	cutting speed (m min^{-1})
f	feed (mm rev^{-1})
α	effective contact length between the flank face and the machined surface (μm)
β	average chip thickness (mm)
PSZ	primary shear zone (chip formation zone)
SSZ	secondary shear zone (chip–workpiece contact zone)
TSZ	third shear zone (tool–workpiece contact zone)
μ_{TSZ}	average friction coefficient on the flank face
μ_{SSZ}	average friction coefficient on the rake face
V_{chip}	chip speed (average sliding velocity on the secondary shear zone) (m min^{-1})
h	undeformed (or uncut) chip thickness (mm)
F_{C1}	tangential force in the secondary shear zone (N)
F_{f1}	normal force in the secondary shear zone (N)
F_{C2}	tangential force in the third shear zone (N)
F_{f2}	normal force in the third shear zone (N)
ϕ_{tot}	total frictional heat flux (W)
ϕ_{pin}	heat flux entering the pin (W)
Λ_3	heat partition coefficient at the tool–workpiece interface (percentage of generated heat flux conducted to the tool)
Λ_1	percentage of the shearing energy transformed into heat
Λ_2	percentage of heat generated in the *PSZ* conducted to the machined surface
$D_{TSZflux}$	heat flux density in the third shear zone (W mm^{-2})
$D_{PSZflux}$	heat flux density in the primary shear zone (W mm^{-2})
b	width of cut (disk thickness) (mm)
μ_{app}	apparent friction coefficient
μ_{adh}	adhesive part of the apparent friction coefficient
μ_{def}	deformation part of the apparent friction coefficient
V_s	local sliding velocity (m min^{-1})
F_n	normal force measured during friction test (N)
F_t	tangential force measured during friction test (N)
k	thermal contact conductance (m^2 K^{-1})
σ_{ZZ}	normal pressure applied in *TSZ* (MPa)
σ_{YZ}	tangential stress applied in *TSZ* (MPa)
a_p	cutting depth (mm)
I–C	indirect tool–workpiece contact zone
D–C	direct tool–workpiece contact zone
H	convection coefficient (W m^{-2} K^{-1})
h_{max}	undeformed (or uncut) chip thickness between the direct contact zone (*D–C*) and the indirect contact zone (*I–C*) (mm)
w	total tool/workpiece contact length along feed direction (mm)
K	tool/workpiece contact length of the indirect contact zone (*I–C*) along feed direction (mm)
d	tool/workpiece contact length of the direct contact zone (*D–C*) along feed direction (mm)

Surface integrity depends on the thermo-mechanical loadings induced by all the previous manufacturing operations, even if the last operation has a major responsibility [9]. Among the finishing operations applied to critical parts, longitudinal finish turning is widely used. So, this article focuses on modeling the residual stresses induced by the finish longitudinal turning of the 15-5PH martensitic stainless steel using a hybrid model. A hybrid model consists in replacing the tool and chip modeling by equivalent loadings (Fig. 1). These equivalent loadings are moved onto the machined surface with a velocity equal to the cutting speed. After the cooling phase, this model makes it possible to predict residual stresses. This hybrid model for residual stress prediction presents advantages like the removal of highly distorted mesh and contact modeling and the possibility of 3D multi-revolution simulations. It is important to note that this model is dedicated to surface integrity prediction (residual stress) and is not adapted to finely model the material flow around the cutting edge for example.

In the literature, experimental studies were performed to quantify the effects of cutting parameters on surface integrity [10–12]. In parallel, various models have been developed. Historically, analytical models were the most popular [13]. Several contributions have improved this work [14]. Ulutan et al. [15,16] have developed a thermo-mechanical model of residual stress generation where both the thermal field of the workpiece and mechanical cutting forces are coupled. Such models enable very fast calculations and facilitate a good understanding of the phenomena involved in residual stress generation. Unfortunately, severe assumptions do not enable to provide quantitative results. Different numerical models have also been developed. Deng and Shet [17] and Salio et al. [18] have used a numerical Lagrangian formulation of the material removal process. However, such models encounter two main difficulties: the separation criterion around the cutting edge radius [19] and the modeling of friction [20]. Moreover Lagrangian models require long calculation times. Some models, similar to the one proposed by Nasr et al. [21], use an Arbitrary Lagrangian Eulerian (A.L.E) formulation providing fast results. These works use an explicit time integration algorithm which leads to difficulties to model the relaxation time (crucial for residual stress prediction). Yang and Liu [22] presented a numerical solution for predicting residual stresses. They highlight the influence of the friction coefficient at the tool/workpiece interface on the residual stresses value.

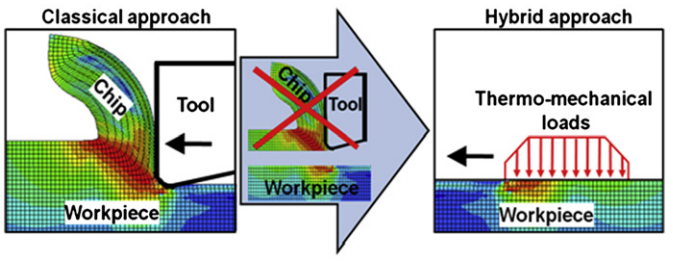

Fig. 1. Hybrid model principle.

An alternative approach proposed by Valiorgue et al. [23] consists in modeling the residual stress generation by removing the chip formation and replacing it with equivalent thermo-mechanical loadings (Fig. 1). Such a model uses an implicit formulation. After the cooling phase, this model enables to predict the residual stresses. This type of approach has been firstly used for residual stress computation during a grinding process [24] and was based on thermal aspects only.

Indeed, during a turning operation, the cutting tool makes a large number of revolutions around the workpiece. The cutting tool modifies the residual stress state obtained during the previous revolution. When machining with low feed and a large nose radius, which is typical in finish turning, it can be assumed that several revolutions are necessary to reach a steady state.

Hence, 2D models are interesting to understand the mechanisms involved during the surface integrity generation, but they are unable to provide quantitative data comparable with practical longitudinal turning operations.

Based on this statement, some researchers started 3D simulations. Sasahara et al. [25] proposed to combine two Lagrangian plane models: an orthogonal cutting simulation containing the cutting direction and an indentation-like simulation of a corner radius into the machined surface (containing the feed direction). A more recent model, proposed by Attanasio et al. [26], uses a Lagrangian formulation (software DEFORM 3D) to predict the residual stress induced during cutting. This work is an important step forward. Nevertheless, the limitation of this Lagrangian formulation has already been mentioned previously and this code does not consider any variation of the friction coefficient along the contact. Finally the calculation time is too long to be compatible with an industrial exploitation.

To deal with the problem of surface integrity prediction, two main questions are recurrent. Firstly, how to quantify the thermo-mechanical impact of the machining process at the level of the final workpiece surface? Secondly, what is the link between the thermo-mechanical loadings induced by the machining process and the final surface integrity (in particular residual stresses)?

Residual stresses are induced by a complex combination of thermal, mechanical and chemical (metallurgical) effects [14,27]. Mechanical effects (pressure and shear stresses) generally provoke compressive residual stresses due to a plastic deformation of the surface material [28,29]. Conversely, thermal effects lead to tensile residual stresses due to important thermal gradients [30,31]. When mechanical and thermal aspects are strongly combined in a process (as in machining), it is very difficult to predict if compressive or tensile residual stresses will be prevailing. In grinding, Chen et al. [30] mention a critical value of temperature: below this transition temperature, residual stresses are compressive ones, above the same temperature, they switch to tensile stresses. In the literature, experimental studies were performed to quantify the effects of cutting parameters on surface integrity. Capello [10] shows that in turning, surface residual stresses can be tensile or compressive depending on process parameters (feed, cutting speed, tool nose radius, etc.) and on the characteristics of the machined material. Changes of cutting conditions lead to a variation of thermo-mechanical surface loadings. This fickleness perfectly illustrates the difficulty to predict residual stress sign and value.

To quantify the surface thermo-mechanical loadings associated with a manufacturing operation (in particular the machining process), different approaches are possible. On one hand, with regard to the thermal aspect, the sub-surface temperature can be directly measured during the process. Then an inverse approach is used for the heat flux identification (shape and intensity) [24,32]. Nevertheless, this approach has not been adapted to the mechanical aspect.

On the other hand, machining thermo-mechanical loadings can be extracted from analytical or numerical models. For example, Ulutan et al. [15] developed a complex analytical model to calculate tool, chip and workpiece temperature fields and cutting force distribution. The results are directly dependent on the cutting conditions. Numerical cutting models are now widely utilized. Lagrangian formulation [17,33] or Arbitrary Lagrangian Eulerian (A.L.E.) model [21] are used. Authors observe the temperature fields and the macroscopic cutting and feed forces [34]. Nevertheless, the surface thermo-mechanical loading as a function of the cutting conditions is never precisely extracted and quantified.

An alternative method, presented in the first part of this paper, consists in quantifying machining thermo-mechanical loadings using combined experimentations and analytical models. This method has been developed in order to predict residual stresses induced by an operation of finish turning using a hybrid model (Fig. 1). Indeed, an important step of equivalent loading calibration is necessary to use a hybrid model. The shapes and intensities of these equivalent thermo-mechanical loadings are estimated by means of preliminary experimental tests: friction tests and orthogonal cutting tests.

Firstly, the method considers an orthogonal cutting configuration (2D) to simplify loadings quantification and interpretation. Then the second part of this paper presents a generalized 3D model of residual stress prediction based on the equivalent thermo-mechanical previously quantified. Finally, the numerical results are compared with the experimental measurements obtained by X-ray diffraction.

2. Equivalent thermo-mechanical quantification in 2D configuration

2.1. Methodology

The following approach is applied to determine the locations, shapes and intensities of loadings equivalent to the machining impact on the workpiece surface (Fig. 2). The first step consists of determining which thermal and mechanical loadings should be taken into account under the cutting zone. Then simple forms are chosen to represent them. To this end, a Finite Element (FE) simulation of orthogonal cutting is used. It is important to note that the aim of this model is not to precisely compute the values of the loadings but to extract their simplified shapes and their locations. Nevertheless, its validity can be checked using a comparison with

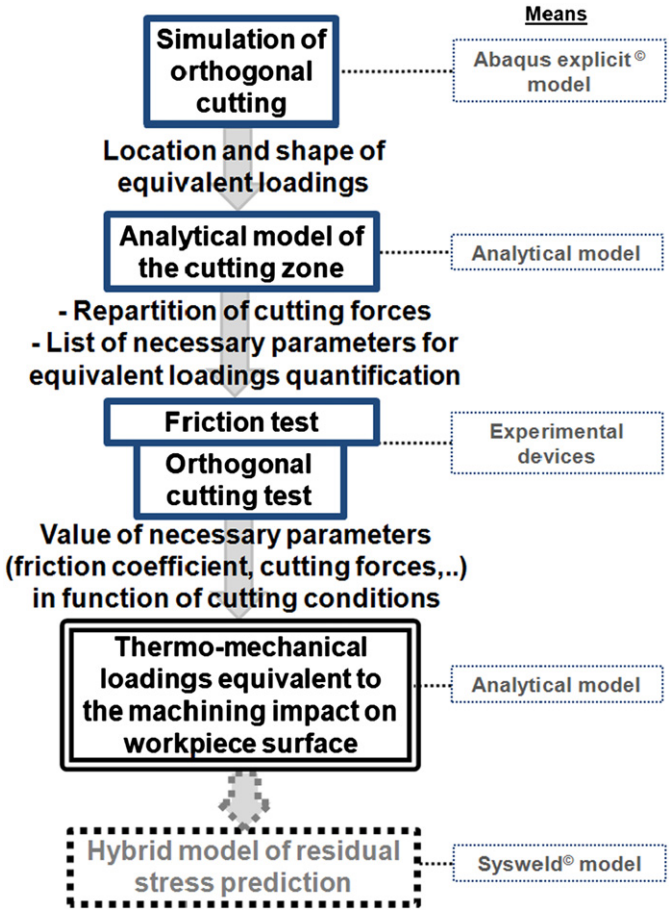

Fig. 2. Methodology to determine and quantify equivalent thermo-mechanical loadings.

experimental data. The second step consists in quantifying equivalent loadings intensity. An analytical representation of the cutting zone is used to distribute forces and heat flux. It appears that various parameters (forces, contact lengths, friction coefficients) have to be measured to achieve loadings quantification.

So equivalent loadings are quantified without using directly a numerical model but using two basic experiments: friction tests and orthogonal cutting tests. This choice is justified because experimentation enables to faithfully include physical phenomena which are difficult to simulate. Moreover, experimental calibration permits to easily take into account a wide range of cutting conditions (cutting speed, feed or change of material).

Hence, the main objective of the first part of this paper is to apply the previously described methodology in the case of the orthogonal cutting of a 15-5PH steel using standard TiCN–Al_2O_3 coated carbide inserts. So the locations and shapes of the equivalent loadings are determined using a numerical 2D orthogonal cutting model. Then, the quantification of loading intensity is achieved by means of preliminary experimental tests: friction tests and orthogonal cutting tests.

The 15-5PH stainless steel is a low-carbon martensite stainless steel containing approximately 3 wt% Cu. It is strengthened by the precipitation of highly dispersed copper particles in the martensite matrix. Several studies have been reported in the literature concerning the microstructural characterization [35] and mechanical behavior of PH stainless steels [36]. Aghaie-Khafri and Adhami [37] provide a complete study on hot deformation and strain rate sensitivity of 15-5PH.

2.2. Identification of equivalent thermo-mechanical loading locations and shapes

2.2.1. A.L.E. orthogonal cutting model

A numerical cutting model is used to obtain heat flow and pressures at the machining surface level. The aim of this model is not to be a predictive model of loading values. Indeed, physical phenomena around the cutting edge are too complex to be finely modeled (in particular the material behavior law in these conditions of pressure, temperature and strain rate) and do not allow to extract accurate quantitative results. Only shapes and locations of surface loadings have been taken into account.

The 2D orthogonal cutting model based on the A.L.E. approach (Fig. 3) has been developed and wholly described by Courbon et al. [38]. The simulated machining time is equal to 10 ms for the following simulations. Coupled thermo-mechanical simulations are conducted in the commercial code Abaqus/Explicit. The model consists of a deformable workpiece and rigid cutting tool. Both solids are meshed using 4-node plane strain thermally coupled quadrilateral elements (CPE4RT). An adaptive meshing technique has been employed. In this Eulerian-based A.L.E. model, Eulerian boundaries, such as input and output surfaces, have to be defined to permit the flow of the workpiece material (Fig. 3). The inflow takes place on the left with the prescribed cutting speed set at the nodes, whereas the outflow is made possible through the upper chip and right-hand surfaces of the workpiece, as specified in Fig. 3. The nodes at the bottom of the workpiece are fixed vertically via symmetry conditions whereas the tool is completely embedded.

As for the interface, a master slave penalty contact method was used. In our reference configuration, the frictional behavior of the interface is modeled according to the identification performed using the friction tests and results described in the sequel. So the friction coefficient is set as dependent on the local sliding velocity. Regarding thermal modeling of the interface, thermal contact conductance k is fixed to $10^4 \times W = m^2\,K^{-1}$ to be consistent with the identification of Guillot et al. [39].

2.2.2. Tool and workpiece specifications

The physical properties of the WC-Co cutting tool substrate and 15-5PH workpiece can be found respectively in Rech et al. [40] and Wu et al. [41] and will not be recalled here. The Al_2O_3–TiCN coating has not been directly represented in the numerical model but its tribological influence at the interface has been taken into account with the friction model (friction and heat partition coefficients).

A Johnson–Cook-Flow stress model Eq. (1) has been used to model the 15-5PH steel mechanical behavior. A, B, n and m parameters, presented in Table 1, have been calibrated using Wu et al. [41] experimental traction tests from 20 °C to 1100 °C. In the literature, there is no data for 15-5PH steel with an important variation of the plastic strain rate, necessary for C parameter calibration. So, C parameter identified for an AISI 4140 steel has been used [42]. This steel has been chosen since its microstructure (martensitic) and its global mechanical properties are similar to the 15-5PH steel

$$\sigma_{eq} = [A + B(\varepsilon_p))^n]\left[1 + C\ln\left(\frac{\dot{\varepsilon}_p}{\dot{\varepsilon}_o}\right)\right]\left[1 - \left(\frac{T - T_o}{T_f - T_o}\right)^m\right] \quad (1)$$

Table 1
Johson–Cook model parameters for 15-5PH.

A (MPa)	B (MPa)	n	C	$\dot{\varepsilon}_o$ [/s]	m	T_m (°C)	T_o (°C)
855	448	0.14	0.0137	1	0.63	1440	20

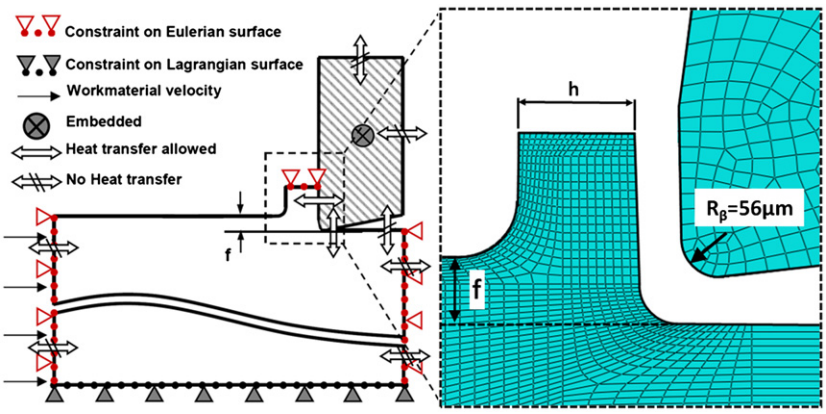

Fig. 3. Description of the ALE model employed.

where A (MPa) is the yield strengh, B (MPa) is the hardening modulus, C is the strain rate sensitivity coefficient, n is the hardening coefficient, m is the thermal softening coefficient, $\dot{\varepsilon}_p$ (s^{-1}) is the plastic strain rate, $\dot{\varepsilon}_o$ (s^{-1}) is the reference plastic strain rate, ε_p is the current plastic strain, T_m (°C) is the melting temperature, T (°C) is the current temperature, and T_o (°C) is the room temperature.

The important thermo-mechanical interactions existing in machining are considered by the Quinney–Taylor coefficient which indicates the fraction of plastic work converted into heat. A constant value of 0.9 has been set as it is usually considered in the machining literature [43].

2.2.3. *Extraction of thermo-mechanical loading shapes and locations at the machined surface level*

The aim of this orthogonal cutting simulation is to locate and extract the shape of the thermo-mechanical loadings at the final surface level (Fig. 4). Three types of loadings are considered: heat flux, normal pressure and tangential stress.

For simulations, standard cutting conditions are considered:

- cutting speed $V_c = 150$ m min^{-1},
- feed $f = 0.1$ mm rev^{-1}.

The simplified shapes of equivalent thermo-mechanical loadings are extracted at the final surface level (Fig. 4). This section aims at presenting the shapes of thermo-mechanical loadings in each zone: below the chip formation zone (primary shear zone: *PSZ*) and in the tool/workpiece contact zone (third shear zone: *TSZ*).

The *PSZ* is assumed to have a sheer thermal influence. Its mechanical influence onto the final workpiece surface is neglected. Indeed, the stress value below the chip formation zone is very low and less than the yield stress of 15-5PH even for high temperatures. Regarding the mechanical loading induced by the chip root (*PSZ*) at the final surface level (illustrated in Fig. 4), the tangential stress varies from 426 MPa ($V_c = 250$ m/min, $f = 0.2$ mm/rev) to 613 MPa ($V_c = 90$ m/min, $f = 0.1$ mm/rev) and the normal stress varies from 448 MPa ($V_c = 250$ m/min, $f = 0.2$ mm/rev) to 244 MPa ($V_c = 90$ m/min, $f = 0.1$ mm/rev). The temperature in this zone reaches a maximum value of 203 °C for these cutting conditions, so the minimum 15-5PH yield stress is 620 MPa. Authors conclude that plastic strain in this zone is null or negligible compared to the stresses/strain in the *TSZ* at the final surface level.

In the *PSZ*, the heat flux density is assumed to be homogeneous. The width of the heat flux is assumed to be equal to the average chip thickness β.

The *TSZ* is considered to have a thermal and mechanical influence. The mechanical pressure is assumed to have a parabolic shape. The width of parabol α corresponds to the distance between the rake face and the end of the tool–workmaterial interface on the flank face.

The friction coefficient is assumed to be constant in the third shear zone. Its value depends on the sliding velocity as shown by Bonnet et al. [44], which is very close to the cutting speed. As a consequence, friction induces a parabolic shear stress in the same zone.

Additionally friction induces a heat flux at the interface, assumed to be homogeneous. Heat is conducted to the cutting tool and to the machined surface. The heat partition coefficient also depends on the sliding velocity as shown by Bonnet et al. [44].

The shapes of these thermo-mechanical loadings are clearly simplified compared with computational results and can easily be criticized. The aim of this simplification is to facilitate the loadings quantification using experiments. Nevertheless, comparisons of predicted residual stress profiles with experimental measurements (Section 2.2) are fully satisfactory for this first approach.

2.3. *Analytical identification of the parameters required for loadings quantification*

After the characterization of equivalent loading shapes and locations, a quantification step has to be carried out. So it is necessary to establish the link between experimentally measurable parameters (in particular cutting, feed forces, friction coefficient and heat partition coefficient) and desired equivalent thermo-mechanical loadings. A simple analytical model is then used. The cutting angle ($-5°$) has been used during orthogonal cutting tests but is not taken into account in force calculations because of its negligible influence ($\cos 5° = 0.996$).

The local cutting forces are calculated by resolving the following system (Fig. 5):

$$F_c = F_{c1} + F_{c2} \tag{2}$$

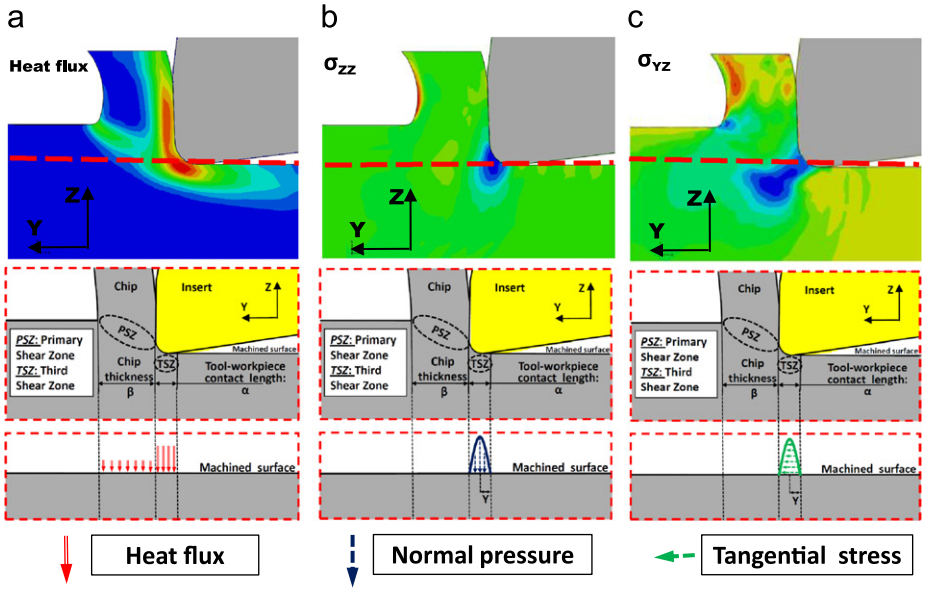

Fig. 4. Comparing the results of orthogonal cutting simulation with chosen equivalent loading shapes for (a) heat flux, (b) normal pressure, and (c) tangential stress.

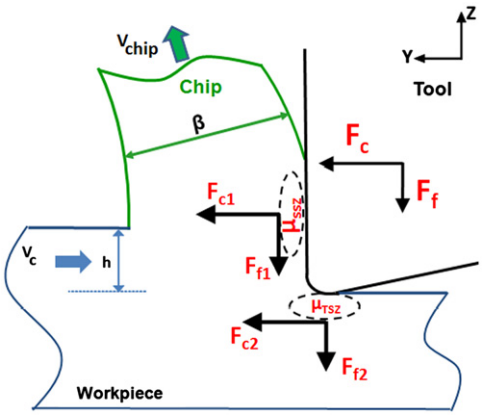

Fig. 5. Analytical model of cutting force distribution.

$$F_f = F_{f1} + F_{f2} \tag{3}$$

$$F_{f1} = F_{c1}\mu_{SSZ} \tag{4}$$

$$F_{c2} = F_{f2}\mu_{TSZ} \tag{5}$$

where μ_{SSZ} is the average friction coefficient on the rake face (*SSZ*); μ_{TSZ} is the average friction coefficient on the flank face (*TSZ*). μ_{TSZ} is the estimated using friction tests. The sliding velocity in the third shear zone is close to the cutting speed. μ_{SSZ} is estimated also with the friction model. The average sliding velocity on the secondary shear zone is estimated by the chip compression ratio:

$$V_{chip} = (V_c h)/\beta \tag{6}$$

where h is the undeformed chip thickness and β is the average chip thickness (Fig. 5).

The normal pressure and tangential stresses applied in the *TSZ* are assumed to have a parabolic shape coming from Hertz contact theory [45] (Fig. 4):

$$\sigma_{ZZ}(y) = \frac{2F_{f2}}{\pi(\alpha/2)^2}((\alpha/2)^2 - y^2)^{1/2} \tag{7}$$

$$\sigma_{YZ}(y) = \mu_{TSZ}\frac{2F_{f2}}{\pi(\alpha/2)^2}((\alpha/2)^2 - y^2)^{1/2} \tag{8}$$

In the *TSZ*, a heat flux is generated by friction. This heat flux source has been assumed to be homogeneous and independent from the contact pressure along the flank face contact. It only depends on the tangential force and sliding speed. The heat flux density is estimated from orthogonal cutting tests by

$$D_{TSZflux} = \frac{F_{C2}V_C}{b60\alpha}(1 - \Lambda_3) \tag{9}$$

where b is the width of cut (disk thickness) and α is the effective contact length between the flank face and the machined surface, and Λ_3 is the heat partition coefficient at the interface (percentage of generated heat flux conducted to the tool).

Concerning the primary shear zone (*PSZ* in Fig. 4) it has been assumed that the heat flux is homogeneous. The heat flux density can be estimated by means of the plastic shearing energy consumed in this zone. A large percentage Λ_1 of this energy is transformed into heat. Additionally, a part of this heat $(1-\Lambda_2)$ is transported with the chip flow whereas the rest Λ_2 is conducted to the machined surface. Hence the heat flux density supported by the machined surface coming from the primary shear zone can be estimated by

$$D_{PSZflux} = \frac{F_{C1}V_C}{b60\beta}\Lambda_1\Lambda_2 \tag{10}$$

where Λ_1 is the percentage of the shearing energy transformed into heat. According to Shi et al. [46], Λ_1 is close to 0.85. Λ_2 is the percentage of heat conducted to the machined surface in the *PSZ*. According to [47], Λ_2 is close to 0.1.

Finally, it is possible to draw up the list of parameters required for loading calibrations:

- Extracted from friction tests:
  - Friction coefficient as a function of the sliding speed (μ_{TSZ}, μ_{SSZ}).
  - Heat partition coefficient at the tool–workpiece interface as a function of the sliding speed (Λ_3).
- Extracted from orthogonal cutting tests:
  - The feed force (F_f).
  - The cutting force (F_c).
  - The average chip thickness (β).
  - The effective contact length between the flank face and the machined surface (α).

2.4. Identification of a friction model adapted to a tool–chip–workpiece interface

2.4.1. Experimental set-up

It is now generally accepted that a constant Coulomb friction coefficient cannot represent the contact at the tool–chip–workpiece interface during the cutting operation because of exceptional mechanical and thermal loadings. In the case of steel machining, usual cutting conditions lead to severe tribological conditions: high velocities (60–600 m/min), high temperatures (up to 1000 °C), high pressures (up to 2 GPa) [48].

In order to identify a physical friction and heat partition model, tribological tests have been conducted on the tribometer already fully presented and validated by several previous works [40,44,49]. Its design is illustrated in Fig. 6. This tribometer reproduces machining friction conditions (velocity and pressure).

The work material is simulated through a cylindrical bar made of 15-5PH steel in precipitation-hardened condition H1025 (40 HRC). The cutting tools are simulated through hemispherical pins (ø17 mm) made of cemented carbide with a grade similar to the one used for cutting tools dedicated to martensitic stainless steel machining (76% WC–11% Co–9% TiC–2% TaC–2% NbC; average grain size ≈ 3 μm). In order to eliminate the potential influence of the surface roughness, the pins were polished to reach a low surface roughness ($Ra < 0.3$ μm), which is coherent with a typical surface roughness on a finely ground carbide cutting tool. The pins were coated with Al_2O_3 (4 μm) on TiCN (7 μm) deposited by medium temperature chemical vapor deposition.

Concerning bars, after each friction test, a cutting tool refreshes the surface ploughed by the pin. A belt finishing operation was also performed in order to obtain a very low surface roughness ($Ra \sim 0.1$ μm) and a constant surface for each test. Each friction test was approximately 20 s and each friction condition was reproduced three times.

The pin is maintained by an instrumented pin holder that quantifies the heat flow ($ø_{pin}$) entering into the pin [49]. It is possible to define the heat partition coefficient Λ_3 as the percentage of heat conducted to the pin in comparison with the total frictional energy (assuming to be fully transformed into heat).

$$\Lambda_3 = \frac{ø_{pin}}{ø_{tot}} \tag{11}$$

where $ø_{pin}$ is the heat flow entering into the pin and $ø_{tot}$ is the total frictional energy (assumed to be fully transformed into heat).

The pin holder is fixed onto a dynamometer in order to provide the normal force F_n and tangential force F_t (macroscopic forces). The normal force F_n is maintained around 1000 N. The apparent friction coefficient is provided by the ratio of the tangential to the

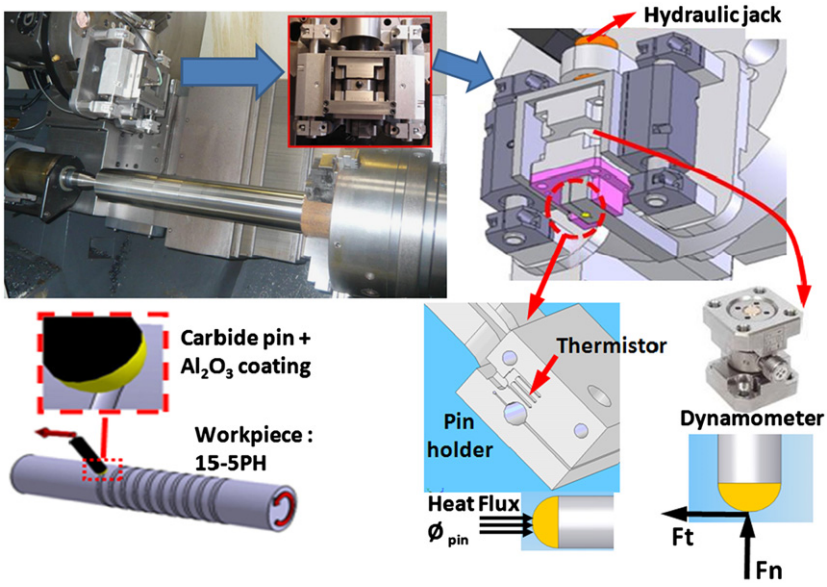

Fig. 6. Design of the tribometer developed.

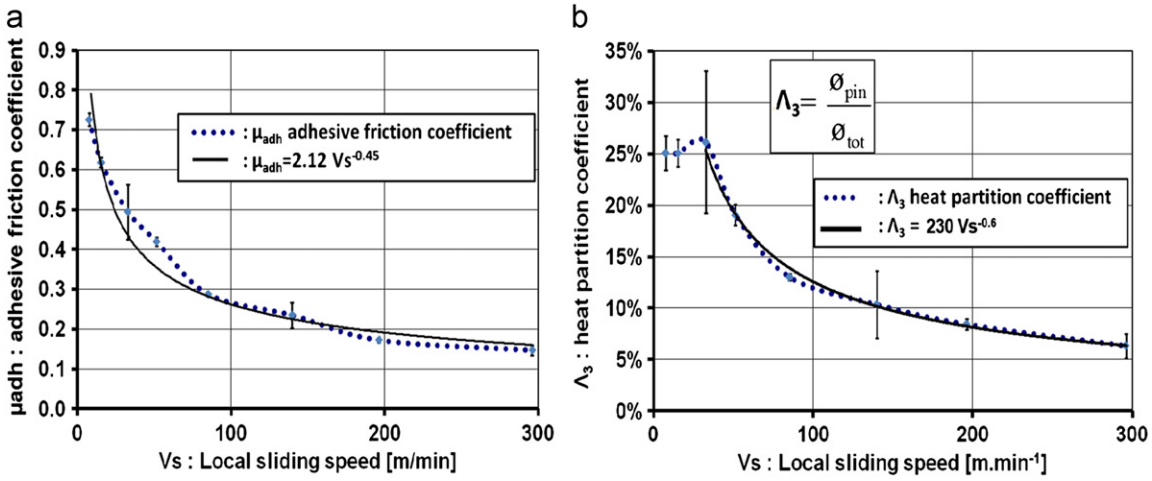

Fig. 7. (a) Adhesive friction coefficient and (b) heat partition coefficient as functions of the local sliding velocity.

normal forces, taken as an average value of the stable zone.

$$\mu_{app} = \frac{F_t}{F_n} \tag{12}$$

The term "apparent" friction coefficient is used because it differs significantly from the "interfacial" friction coefficient. In this work, it is assumed that adhesion is the main friction mechanism at the pin–work material interface. Indeed, the macroscopic forces measured by the tribometer include the friction phenomena (adhesion) and the plastic deformation of the work material, which cannot be neglected under such severe contact conditions ($F_n \approx 1000$ N).

The apparent friction coefficient μ_{app} could be decomposed into two components; see [50]:

$$\mu_{app} = \frac{F_t}{F_n} = \mu_{adh} + \mu_{def} \tag{13}$$

where μ_{app} is the apparent friction coefficient, μ_{adh} is the adhesive part, and μ_{def} is the deformation part.

To extract the part of adhesion and deformation from the apparent friction coefficient, it is possible to numerically post-treat experimental data via a 3D ALE model of the frictional test using the methodology entirely described by Bonnet et al. [44].

2.4.2. Friction test results

Friction test experimental results (normal and tangential forces and heat flux) are post-treated using the friction model previously presented. So, using the methodology developed and described by Bonnet et al. [44], it is possible to extract a heat partition coefficient model and an adhesive friction coefficient model as functions of the local sliding velocity. Fig. 7 presents these two models.

The adhesive friction coefficient is represented by the following equations:

$$\mu_{adh} = 2.12 V_s^{-0.45} \text{ with } 10\,\text{m}\,\text{min}^{-1} < V_s < 300\,\text{m}\,\text{min}^{-1} \tag{14}$$

$$\mu_{adh} = 0.15 \text{ with } V_s > 300\,\text{m}\,\text{min}^{-1} \tag{15}$$

The heat partition coefficient is represented by the following equations:

$$\Lambda_3 = 25\% \text{ with } V_s > 300\,\text{m}\,\text{min}^{-1} \tag{16}$$

$$\Lambda_3 = 230 V_s^{-0.63}\,\% \text{ with } 50\,\text{m}\,\text{min}^{-1} < V_s < 300\,\text{m}\,\text{min}^{-1} \tag{17}$$

$$\Lambda_3 = 6\% \text{ with } V_s > 300\,\text{m}\,\text{min}^{-1} \tag{18}$$

2.5. Orthogonal cutting tests

2.5.1. Experimental procedure

Orthogonal cutting tests have been conducted in order to extract the feed force (F_f), the cutting force (F_c), the average chip thickness (β) and the effective contact length between the flank face and the machined surface (α).

Fig. 8 illustrates the experimental set-up. 3 mm thick disks were cut using a 16 mm wide tool to ensure the validity of the plane strain hypothesis as much as possible. Experiments have been carried out over a range of cutting speeds [90–250] m min^{-1} and feeds [0.05–0.25] mm rev^{-1}. A standard Al_2O_3–TiCN coated carbide insert has been employed.

The cutting force F_c (tangential to the disk radius) and the feed force F_f (radial direction) have been measured by means of a three-component piezoelectric dynamometer. For each configuration, cutting force measurements have been conducted three times. The deviations of the values are lower than 5%. Average values are presented in Fig. 9.

All data concerning the chip morphology and the tool–workpiece contact length have been optically measured. Chips have been coated with resin, polished and etched. The average chip thickness β has been calculated as the average value of the maximum and minimum chip thicknesses (Fig. 8).

2.5.2. Results of orthogonal cutting tests

The cutting force increases in proportion with the feed (and chip section) (Fig. 9a). The feed force also augments with the feed but, contrary to the cutting force, the increase is not directly proportional (Fig. 9b). The cutting and feed forces are reduced by

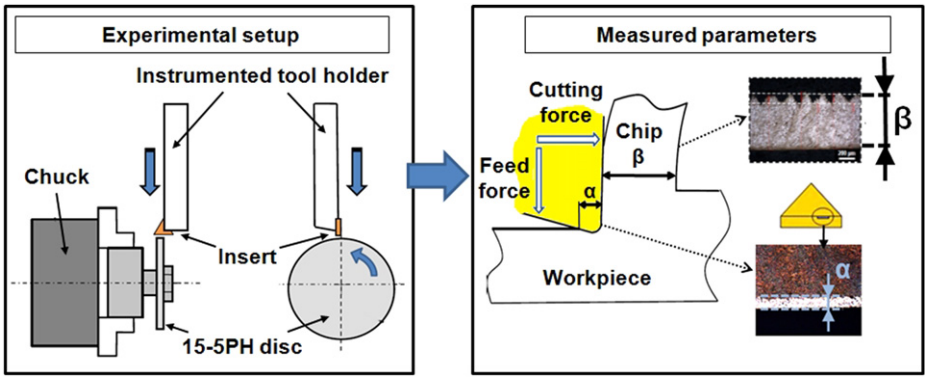

Fig. 8. Orthogonal cutting tests—experimental setup.

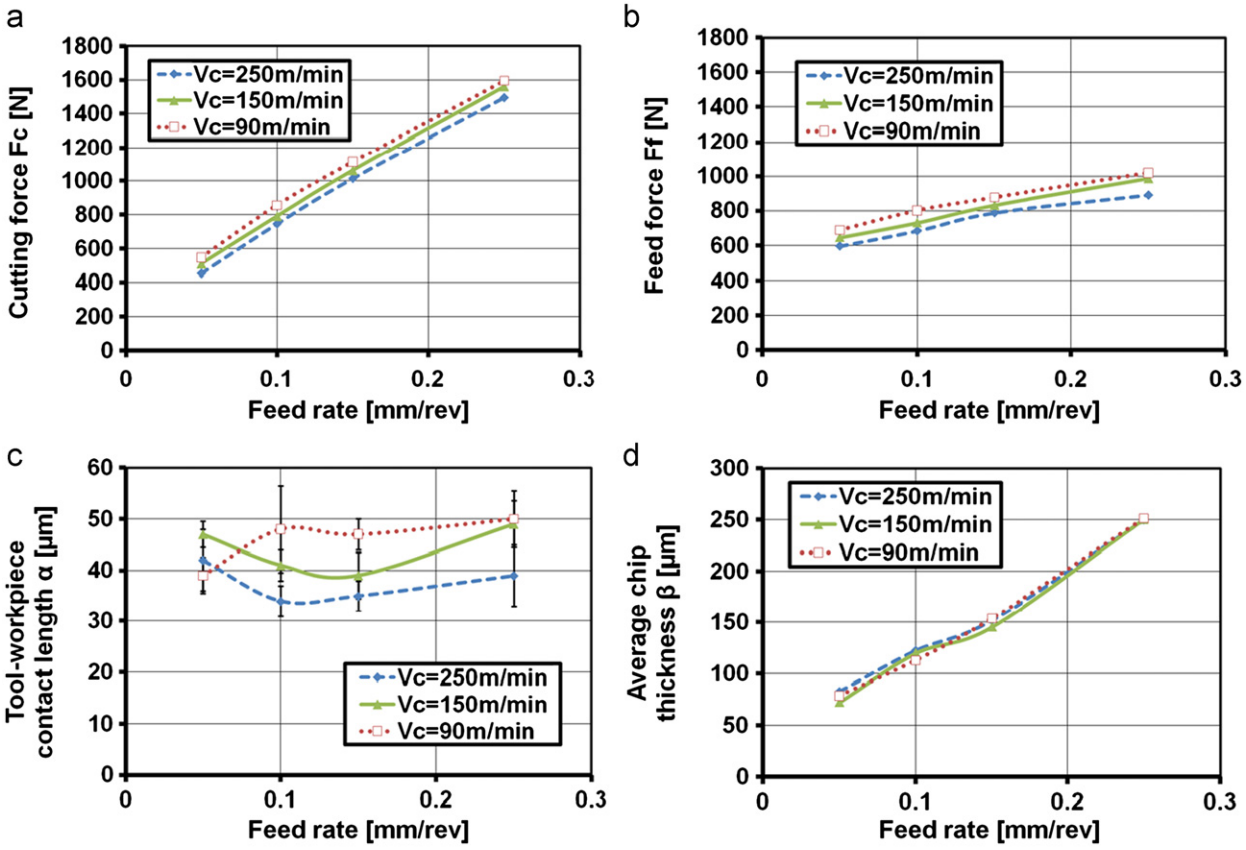

Fig. 9. Orthogonal cutting test results as functions of the feed and the cutting speed: (a) cutting force (F_c), (b) feed force (F_f), (c) effective contact length between the flank face and the machined surface (α), and (d) average chip thickness (β).

6% and 13%, respectively, with the increase in the cutting speed (from 90 to 250 m min^{-1}). Except for a feed of 0.05 mm rev^{-1}, the tool–workpiece contact length increases when the cutting speed is reduced (Fig. 9c). Nevertheless, deviations are significant. The tool–workpiece contact length seems to be practically independent from the feed. Logically the average chip thickness increases with the feed but there is no proportionality (Fig. 9d). Indeed, the chip thickness is 1.5 times as high as the feed (=uncut chip thickness) for f=0.05 mm rev^{-1} whereas the ratio tends to one for f=0.25 mm rev^{-1}.

2.6. Equivalent thermo-mechanical loading values

Using the methodology previously described, the cutting process impact on the final workpiece surface can be evaluated. Equivalent thermal and mechanical loadings can be characterized. So, it is possible to compare their evolutions according to the feed and cutting speed variations.

Table 2 shows that a feed increase has a direct impact on the thermal and mechanical loading of the final work piece surface. The augmentation of the cutting and feed forces due to the increase in the chip thickness leads to an important rise of the normal pressure and tangential stresses (+18% from 0.1 mm rev^{-1} to 0.25 mm rev^{-1}). Similarly, the heat flux augments in the *TSZ* in particular (+18% from 0.1 mm rev^{-1} to 0.25 mm rev^{-1} with regard to the density or the global heat flux conducted).

Observations are different considering an increase in the cutting speed. Indeed, mechanical and thermal loadings do not follow the same trend. This difference is due to the opposition of various phenomena. On one hand, the augmentation of the cutting speed decreases the cutting force, feed force and friction coefficients at the tool/workpiece and tool/chip interfaces. This leads to a decrease in the normal pressure and the tangential stresses of 24% and 52% respectively when the cutting speed varies from 90 m min^{-1} to 250 m min^{-1}. One the other hand, the heat flux generated by friction is directly proportional to the speed of the sliding surfaces. So, the heat flux density in the *TSZ* and *PSZ* increases by 44% and 166% respectively when the cutting speed varies from 90 m min^{-1} to 250 m min^{-1}.

As a conclusion, it is important to note that, regardless of the cutting conditions, the *TSZ* heat flux density is four to six times as high as the *PSZ* heat flux density. This observation corresponds to the numerical cutting model results. Finally, when you are interested in the machining impact on the workpiece surface, the *TSZ* loadings are logically primary compared with the influence of the chip formation zone (*PSZ*). The final surface integrity will practically exclusively depends on the phenomena occurring in the tool/workpiece contact zone (friction, pressure, heat generation, etc.).

2.7. Discussion

Finally, in the present section, a methodology is proposed to quantify the thermal and mechanical impact of the machining process on the final surface of the workpiece.

The developed methodology is easily adaptable to other cutting conditions and materials. Indeed only friction and orthogonal cutting tests have to be performed again to consider another range of machining conditions for example. It is easily transposable to investigate the impact of wear or lubrication conditions on the surface loadings or to compare different workmaterials.

Nevertheless, the quantification of surface thermo-mechanical loadings is not the final aim of the approach. These loadings will be used in a 3D hybrid numerical model dedicated to residual stress prediction after a longitudinal turning operation. This step is developed in the second part of this article. Moreover, equivalent loadings quantified in this way could be utilized for the study of any other surface integrity aspect (metallurgical transformation for example).

3. 3D numerical prediction of residual stresses

3.1. Numerical model design

The model aims to simulate residual stress generation on a cylinder machined by a finish longitudinal turning operation (Fig. 10). As mentioned previously, the proposed method does not consider the chip removal mechanisms. The machined part considered is a cylinder (Fig. 10). Moreover the cutting conditions are constant all along the surface, so it is possible to model a small volume of the cylinder only. Finally, for a large diameter of the cylinder, the machined surface can be considered to be flat. Hence, it becomes possible to model the residual stress generation in finish longitudinal turning by means of a parallelepiped (Fig. 10). The dimensions of the parallelepiped (1.5 mm × 2.3 mm × 0.8 mm) make it possible to simulate several turning revolutions. Five sides of this parallelepiped need to be in contact with the rest of the workmaterial. A large border of a perfectly elastic material (to reduce calculation duration) is positioned around the central parallelepiped (Fig. 11). So, difficulties related to thermal and mechanical boundary effects are minimized and the real material stiffness is simulated. Five sides of the parallelepiped are in contact with the rest of the workmaterial and heat exchanges are possible. The machined surface can also exchange heat with the ambient air (or with an emulsion flow in lubricated condition, $h=10^5$ W m^{-2} K^{-1} according to [51]). As presented in Fig. 11, a quadrangle linear mesh is applied and its size has been optimized in order to minimize the calculation duration without disturbing the result accuracy. A fine mesh is necessary on the machined surface (0.003 mm, 0.4 mm,

Table 2
Model parameters according to cutting speed and feed variations.

	α: Contact length on flank face (mm)	β: Chip thickness (mm)	F_c: Global cutting force (N)	F_f: Global feed force (N)	μ_{TSZ}: Friction coefficient in *TSZ*	μ_{SSZ}: Friction coefficient in *SSZ*	A_3: Heat partition coefficient	Peak normal pressure (MPa)	Peak tangential stress (MPa)	Heat flux density in *PSZ* (W mm^{-2})	Heat flux density in *TSZ* (W mm^{-2})
V_c=150 m min^{-1}											
f=0.1 mm tr^{-1}	0.04	0.11	793	730	0.26	0.23	0.25	5971	1573	399	2325
f=0.15 mm tr^{-1}	0.04	0.155	1063	831	0.26	0.23	0.25	6453	1700	397	2513
f=0.25 mm tr^{-1}	0.04	0.252	1560	986	0.26	0.22	1.00	7062	1861	402	2750
f=0.2 mm tr^{-1}											
V_c=90 m min^{-1}	0.035	0.155	1113	877	0.28	0.28	0.12	7150	2001	250	2003
V_c=150 m min^{-1}	0.04	0.155	1063	831	0.22	0.23	0.09	6390	1421	409	2457
V_c=250 m min^{-1}	0.047	0.155	1013	787	0.18	0.18	1.00	5463	965	665	2883

0.0125 mm), where the thermo-mechanical loadings are applied and lead to strong residual stress gradients. On the contrary, larger meshes are used below the surface. The material is not considered to be free of residual stresses before the turning operation. X-ray diffraction measurements have shown an initial residual stress field of −200 MPa in both axial and tangential directions at the machining depth. This pre-stressing operation is taken into account in the simulations (Fig. 11).

3.1.1. Technological parameters

The cutting tool is a TiCN–Al_2O_3 coated carbide insert. The nominal cutting speed V_c is 150 m min^{-1}. An experimental sensitivity study of the cutting speed has been carried out (in the range of 50–300 m min^{-1}). It shows that it is not an influential parameter in these turning conditions (Fig. 12). So, the sensitivity of the model to the cutting speed has not been developed in the sequel.

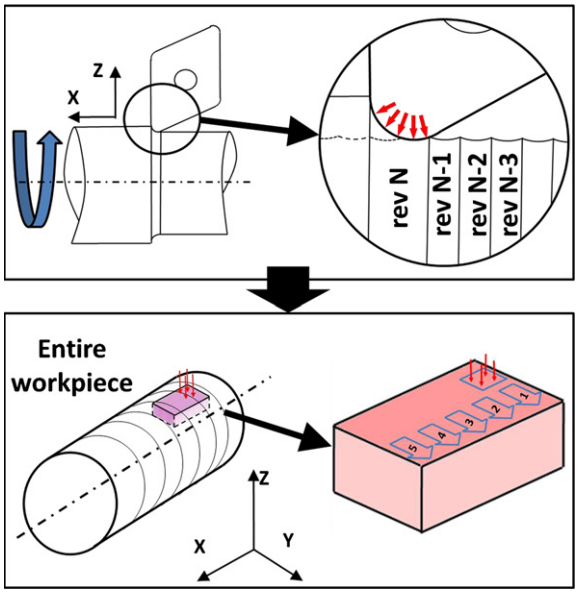

Fig. 10. 3D hybrid modeling strategy.

The nominal feed f is 0.18 mm rev^{-1}. A variation in the range of 0.1–0.3 mm rev^{-1} has been performed for the sensitivity study. The cutting depth a_p is 0.6 mm.

The workmaterial is a 15-5PH martensitic stainless steel cylinder in precipitation-hardened condition H1025 (40 HRC). Its diameter is 175 mm.

3.1.2. Workmaterial mechanical and thermal properties

The 15-5PH stainless steel properties have been extracted from studies of Wu [36] who provides flow stress curves and thermo-mechanical properties from 20 °C to 850 °C. So, a thermo–elasto-plastic behavior with an isotropic hardening is modeled. Further details are available in part one of this article.

Contrary to austenitic stainless steel, a phase transformation may occur during the heating of a martensitic stainless steel. Wu [36] shows that the austenitic phase transformation starts at AC_1 = 665 °C at a heating rate of 2 °C s^{-1}. For this first attempt, the numerical model does not take phase transformations into account. Soft cutting conditions have been chosen in order to avoid material phase change (austenitic transformation) during the machining operation. The results of numerical simulation predict a maximum temperature of 620 °C during turning. This temperature is below the austenitic start temperature and reinforces the assumption to ignore phase changes.

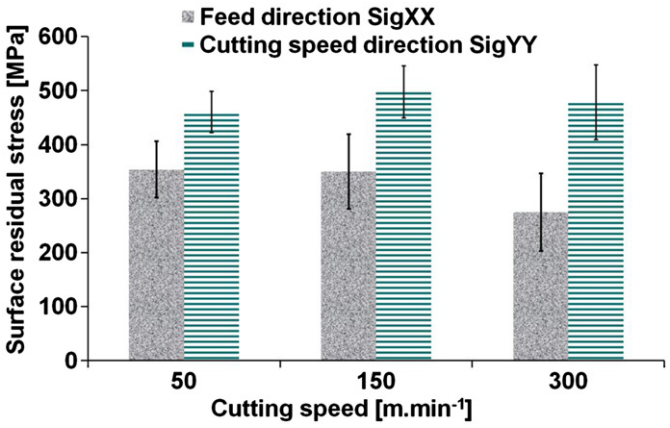

Fig. 12. Influence of the cutting speed on the surface residual stresses.

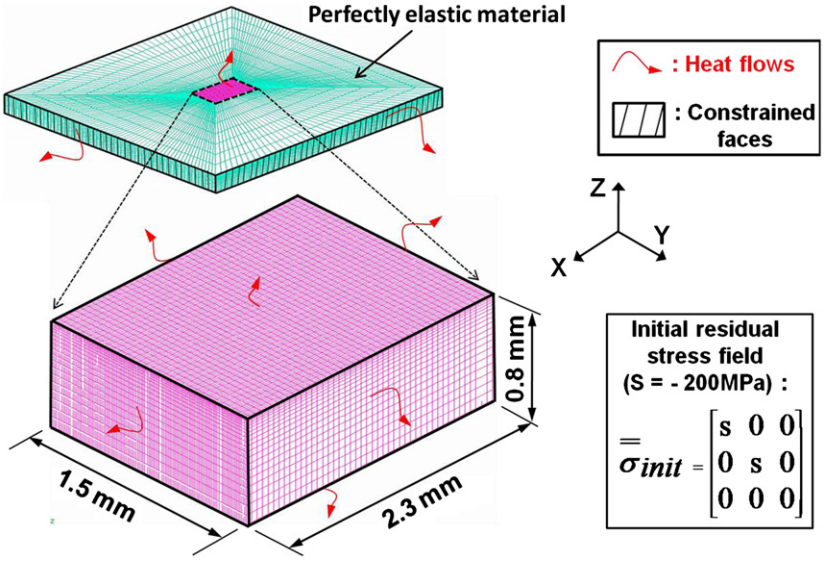

Fig. 11. 3D model geometrical parameters.

3.1.3. 3D thermo-mechanical loading distribution shapes

The method is based on the application of equivalent thermo-mechanical loadings simulating the influence of the *PSZ* and the *TSZ* (Fig. 13). Loading shapes and quantification in 2D orthogonal cutting conditions (Fig. 13, section A) have been fully described in the first part of this article.

This section aims at presenting the shapes of thermo-mechanical loadings along the feed direction in order to obtain three dimensional loadings. So, section B (Fig. 13) is considered.

3.1.3.1. In section A. The shape of the thermo-mechanical loadings in section A is described in the first part of this article.

3.1.3.2. In section B. From Fig. 13, it is necessary to distinguish two zones:

- a zone where the tool is directly in contact with the machined surface (zone *D–C*, Section B),
- a zone where the cutting tool is not in contact with the future machined surface (zone *I–C*, Section B). It is only in contact with the "section to be removed during the next revolution". The influence of the cutting tool is only indirect.

In the primary shear zone (section B), the heat flux conducted to the machined surface is assumed to depend on the radial uncut chip thickness h. In zone *D–C*, the radial uncut chip thickness h varies continuously from 0 to h_{max}. In zone *I–C*, the radial undeformed chip thickness varies continuously as well. Its value may also be larger than in zone *D–C*. However, its influence on the machined surface is only indirect. In this first version of the model, it has been assumed that the heat flux coming from this zone has also a triangular shape in the *X–Z* plane. The width of each zone depends on the geometry of the uncut section.

In the third shear zone (section B), it is assumed that the heat flux has a homogeneous shape in zone *D–C* because of the direct contact between tool cutting edge and workmaterial surface, whereas it has a triangular shape in zone *I–C* to model the presence of the intercalated layer.

The shapes of these thermo-mechanical loadings can easily be criticized. Based on more realistic 3D finite element models of the material removal process, it would be possible to improve these assumptions. However, this work only aims at proposing a first version of a 3D model and to compare results with experimental values.

3.1.4. Estimation of the thermo-mechanical loading intensity

The quantification of thermo-mechanical loading intensity has been fully described in the first part of this article. Orthogonal cutting tests and friction tests are used. Nevertheless, loadings are quantified in section A and have to be extended to section B to obtain 3D loadings (Fig. 13). So, other geometrical parameters need to be estimated:

- w: total tool/workpiece contact length in section B.
- K: tool/workpiece contact length of the indirect contact zone (*I–C*) in section B.
- d: tool/workpiece contact length of the direct contact zone (*D–C*) in section B.
- h_{max}: radial uncut chip thickness between the direct contact zone (*D–C*) and the indirect contact zone (*I–C*).

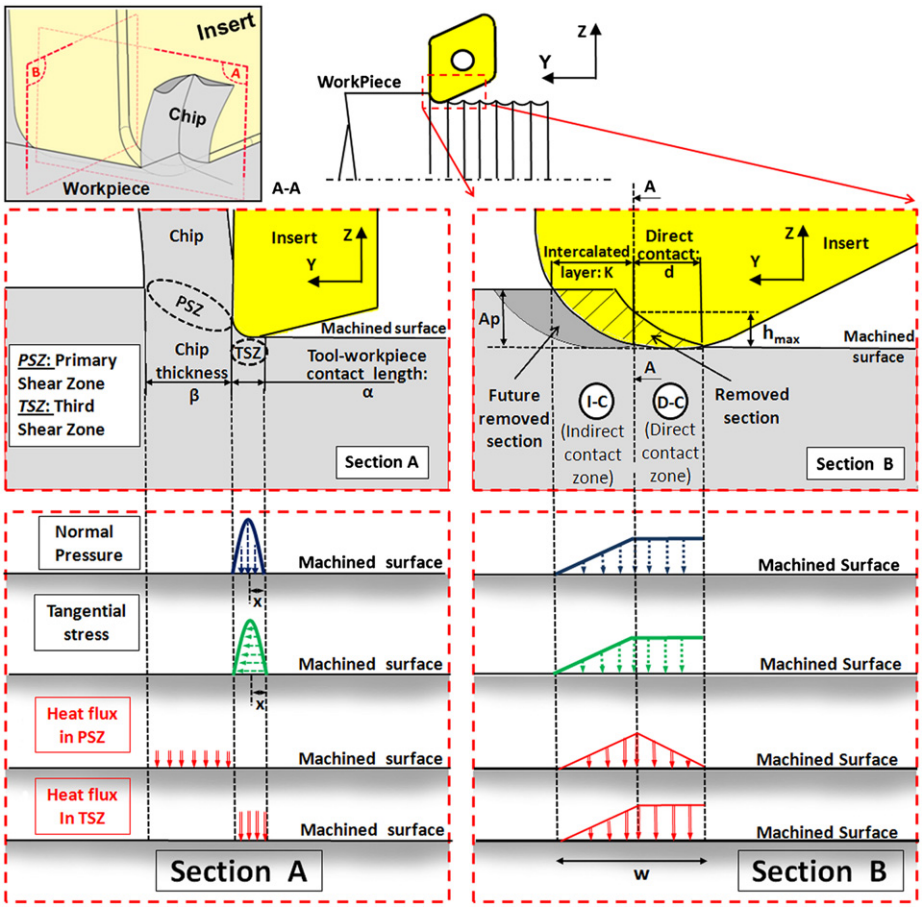

Fig. 13. Thermo-mechanical loadings at the "tool–machined surface" interface.

All these geometrical parameters are directly extracted from drawings of section B, Fig. 13 with the true dimensions of the tool and the cutting depth. These drawings can be made using a CAD software for example.

3.1.4.1. Application of the equivalent thermo-mechanical loadings on the 3D model. The workpiece is modeled as a parallelepiped (Fig. 14). *TSZ* loadings are applied on a rectangular surface having a dimension of w by α. *PSZ* loadings are applied on a rectangular surface having a dimension of w in the feed direction and β in the cutting direction. These loadings are moved in the Y direction (cutting direction) with a velocity equal to the cutting speed. The time t_{cut}, necessary to cross the parallelepiped, is

$$t_{cut} = L_1/V_c \tag{19}$$

Then a cooling period t_{cool} is necessary to simulate the movement of the cutting tool around the workpiece. Its value depends on the diameter of the workpiece D and on the cutting speed V_c,

$$t_{cool} = (\pi D - L_1)/V_c \tag{20}$$

Then a second movement of the thermomechanical loadings is simulated (Fig. 14b). The second movement is shifted in the direction X (feed direction) in order to simulate the feed per revolution of the cutting tool. Due to the fact that the width of the loaded zone w is larger than the feed f, the thermo-mechanical loading affects a part of the surface which has already been affected during the previous revolution (Fig. 14b).

Then the simulation goes on with a second cooling phase and a third application of the thermo-mechanical loadings, and so on.

In the present work, seven revolutions are simulated since it will be shown later that it is sufficient to reach a steady state. At the end of the simulation, the material is cooled down to room temperature and the residual stresses are evaluated.

Approximately 5 h of calculation is necessary with a 3 GHz processor and 8Go RAM computer, which is very fast for the simulation of seven part revolutions.

3.2. Numerical results

The model has been applied to simulate the finish turning of a 15-5PH stainless steel with a TiCN–Al_2O_3 coated carbide tool under the following conditions:

- Cutting speed, $V_c = 150$ m min^{-1}.
- Three feeds: $f = 0.1$, 0.18 and 0.3 mm rev^{-1}.
- Cutting depth, $a_p = 0.6$ mm.

3.2.1. Values of 3D thermo-mechanical loadings

Using the method previously described for the quantification of thermo-mechanical loadings, parameter values (presented in Table 3) have been obtained for the machining conditions studied.

The average chip thickness β, the total loading width w, the direct length d and the indirect contact length K are directly impacted by the feed variations. On the contrary, the contact length of the flank face α remains nearly stable. This parameter is mostly influenced by the cutting edge geometry (constant in our case). The peak normal pressure and the peak tangential stress increase significantly with the feed. This conclusion is the same with regard to the heat flux density.

3.2.2. General observations

Applying the thermo-mechanical loadings previously described, the results presented in Figs. 15 and 16 are obtained.

Fig. 15 presents the residual stresses σ_{xx} and σ_{yy} along the "measurement line" at the surface of the meshed body. This line crosses the parallelepiped in its center so as to be far from its boundaries. The direction Y is parallel to the cutting speed, whereas the direction X is parallel to the feed. It shows the residual stress state after each revolution from the 1st to 7th. It reveals that the residual stress state induced after seven revolutions is not homogeneous either in the Y direction or in the X direction. Residual stresses along the measurement line are periodic. The period corresponds to the feed f. Fig. 15 also shows

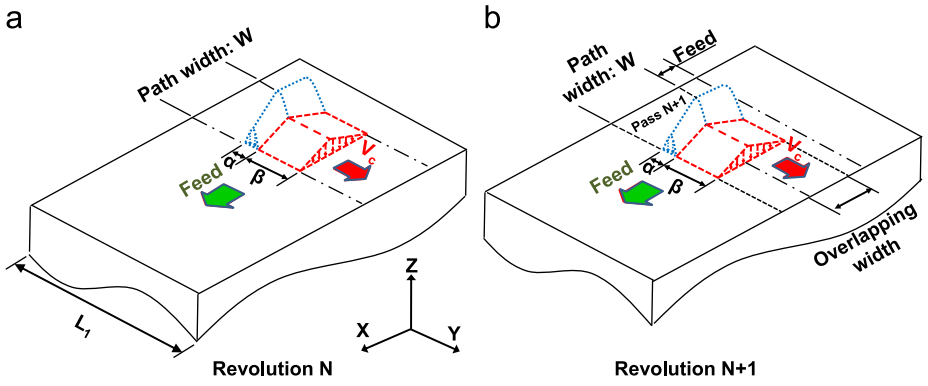

Fig. 14. 3D simulation strategy.

Table 3
Parameter values of the thermo-mechanical loadings for different cutting conditions: $V_c = 150$ m min^{-1}, $a_p = 0.6$ mm, $f = 0.1$, 0.18 and 0.3 mm tr^{-1}.

	α: Contact length on flank face (mm)	β: Chip thickness (mm)	w: Total loading width (mm)	d: Direct contact length (mm)	K: Indirect contact length (mm)	Peak normal pressure (MPa)	Peak tangential stress (MPa)	Heat flux density in *PSZ* (W mm^{-2})	Heat flux density in *TSZ* (W mm^{-2})
$f = 0.1$ mm tr^{-1}	0.04	0.04	1.07	0.1	0.97	3858	858	320	1483
$f = 0.18$ mm tr^{-1}	0.04	0.06	1.14	0.18	0.96	4157	924	366	1598
$f = 0.3$ mm tr^{-1}	0.04	0.1	1.18	0.3	0.88	4481	997	405	1723

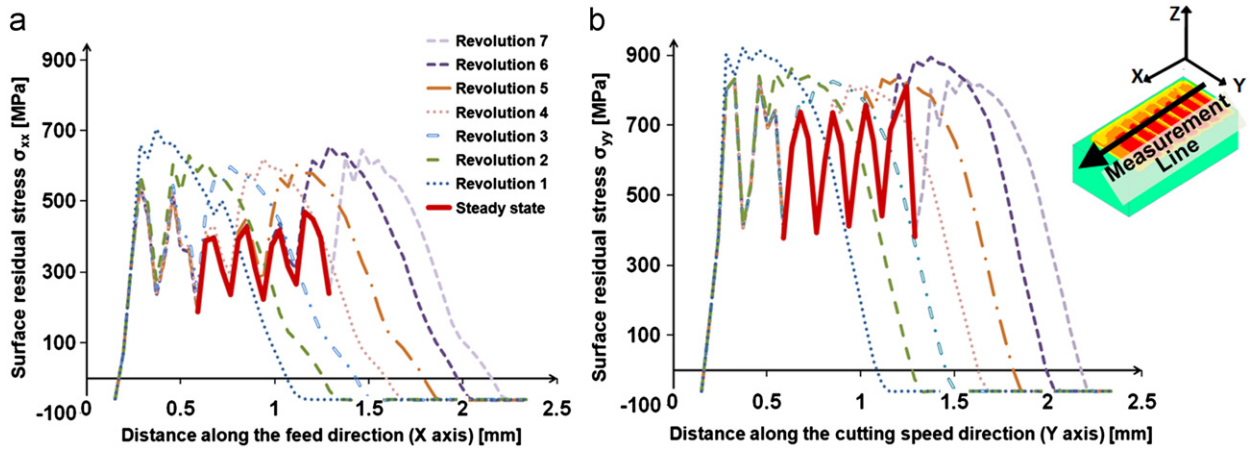

Fig. 15. Evolution of residual stresses on the surface along a measurement line for seven revolutions: (a) along the feed direction=X axis; (b) along the cutting speed direction=Y axis. (V_c=150 m min^{-1}, f=0.18 mm rev^{-1}, a_p=0.6 mm).

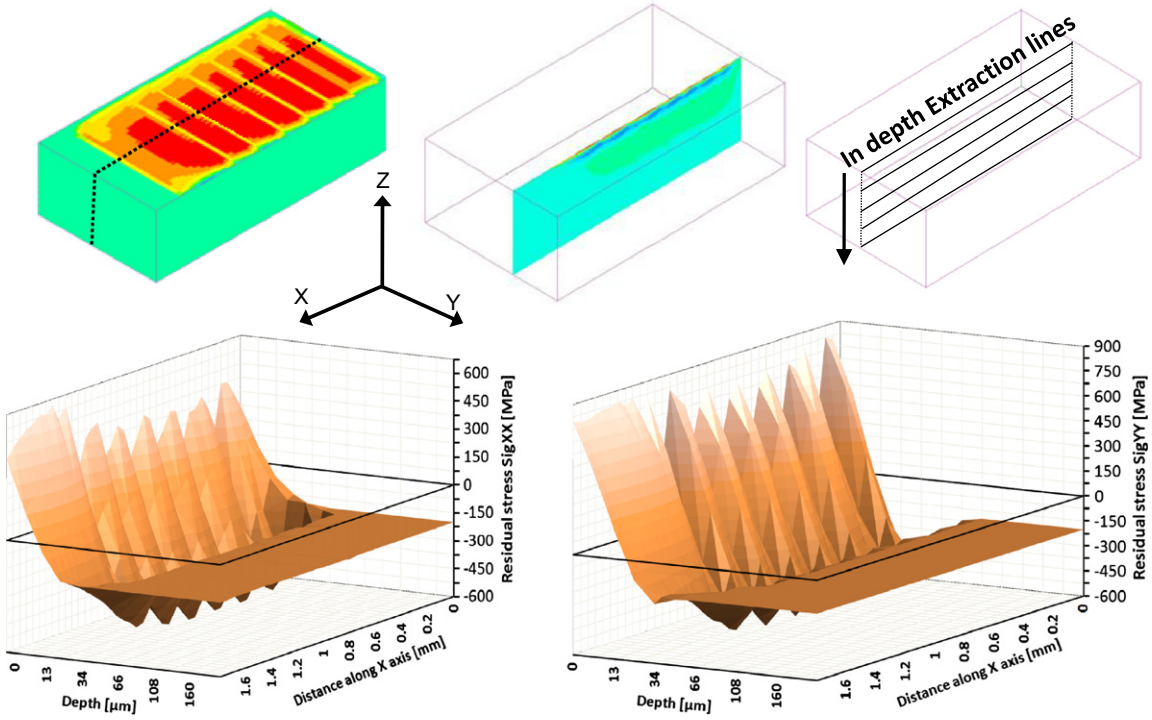

Fig. 16. Residual stress mapping (V_c=150 m min^{-1}, f=0.18 mm rev^{-1}, a_p=0.3 mm).

that three revolutions at least are necessary to obtain a steady state with such cutting conditions. By observing the residual stress state obtained after a revolution, it is noted that the curves are modified by the following revolutions. The periodic variation of residual stresses and the interaction between each path are two key results showing the limitations of 2D models which are unable to highlight such phenomena.

Fig. 16 plots residual stress maps in depth. Due to the variation of residual stresses along the X axis, a 3D map is obtained. When analyzing residual stresses below the surface, it becomes difficult to compare all the curves obtained for various conditions. Hence it has been decided to calculate the average value in the steady state as shown in Fig. 17.

Fig. 18 shows the average values calculated for each depth. It appears that tensile residual stresses are obtained in the external layer. The average surface residual stress is 502 MPa in the feed direction (σ_{xx}) and 552 MPa in the cutting direction (σ_{yy}). A compression peak (-320 MPa) is obtained at a distance around 0.04 mm from the surface. The affected depth is about 0.07 mm.

3.2.3. *Influence of cutting conditions*

Fig. 19 presents average residual stress profiles calculated for the three feeds (0.1, 0.18 and 0.3 mm rev^{-1}), V_c=150 m min^{-1} and a_p=0.6 mm. It appears that the feed does not significantly influence residual stress profiles in the cutting speed direction (σ_{xx}). The difference in the calculated external residual stress is only 160 MPa for f=0.1 mm rev^{-1} and 0.3 mm rev^{-1}. The affected depth is nearly the same for each feed (0.07 mm). Only the compression peak for f=0.1 mm rev^{-1} is significantly reduced. On the contrary, the feed seems to modify the residual stress profile in the feed direction (σ_{yy}) essentially. A larger feed increases the affected depth and the external residual stress varies from 346 MPa to 714 MPa for f=0.1 mm rev^{-1} and 0.3 mm rev^{-1}.

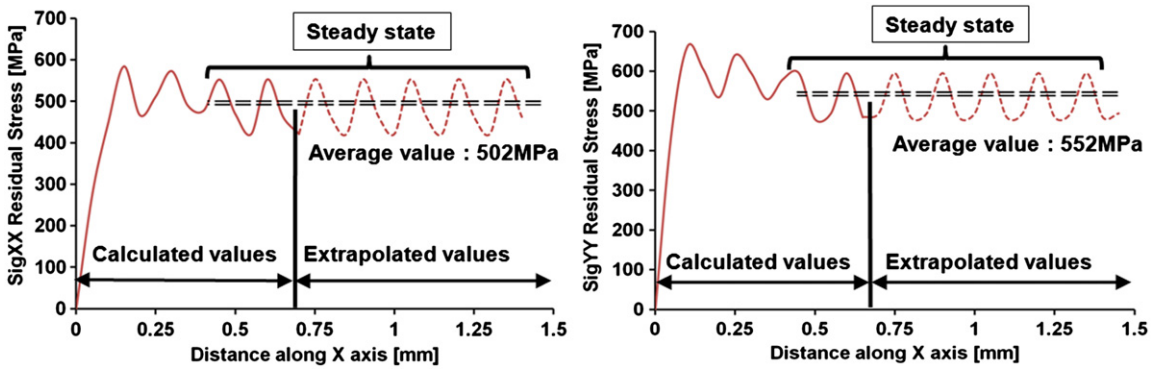

Fig. 17. Evolution of the σ_{xx} and σ_{yy} surface residual stresses on the external surface ($Z=0$).

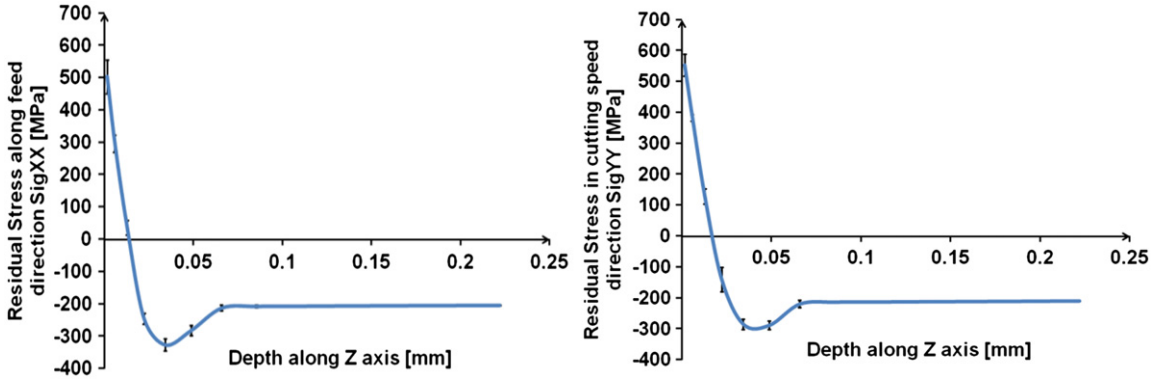

Fig. 18. Calculated residual stress profiles in the X and Y directions ($V_c=150$ m min^{-1}, $f=0.18$ mm rev^{-1}, $a_p=0.6$ mm).

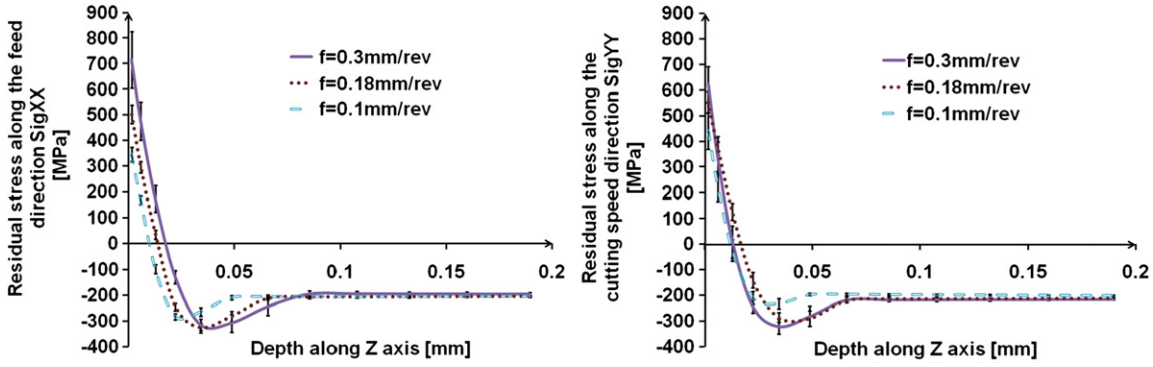

Fig. 19. Residual stress profiles for various feeds.

3.3. Experimental characterization

3.3.1. Measuring set-up

Numerical results will now be compared with experimental measurements obtained by X-ray diffraction. Cylindrical parts have been turned with the same cutting tools and cutting conditions previously presented. The 15-5PH bar is 175 mm in diameter.

The X-ray measurements have been performed with a XRD system provided by the PROTO company, using a MGR40 head and equipped with a 2-mm diameter collimator.

Diffraction conditions:

- Cr Kα radiation with 18 kV, 4 mA.
- $\lambda=0.229$ nm, planes {211}.
- Bragg's angles: $2\theta=155.00^{\circ}$.
- Ω acquisition mode.

Acquisition conditions:

- 7 β-angles (from -30° to $+30^{\circ}$) in both directions X and Y.
- β oscillations: $\pm 6^{\circ}$.

Stress calculation:

- Elliptic treatment method.
- Radio crystallographic elasticity constants:

$$1/2\,S_2 = 5.92 \times 10^{-6}\,\mathrm{MPa}^{-1}$$
$$S_1 = -1.28 \times 10^{-6}\,\mathrm{MPa}^{-1}$$

The in-depth residual stress distribution has been investigated after successive layer removal by means of an electrochemical polishing system.

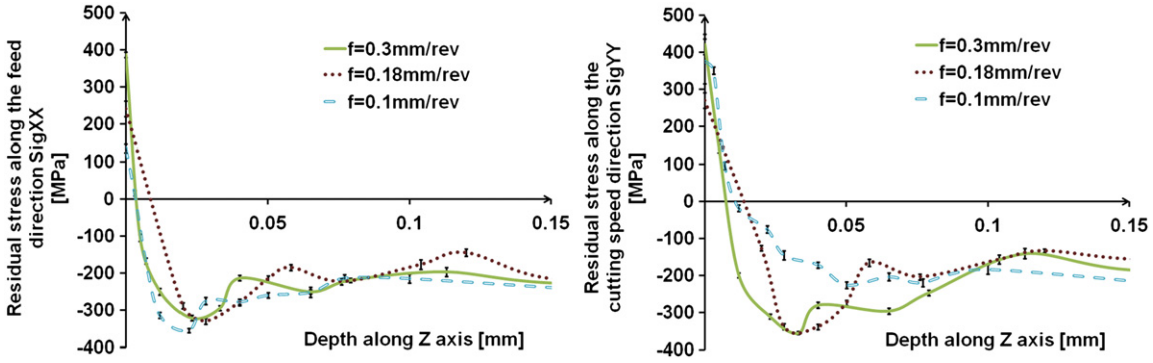

Fig. 20. Measured residual stress profiles for various feeds (V_c=150 m min^{-1} and a_p=0.6 mm).

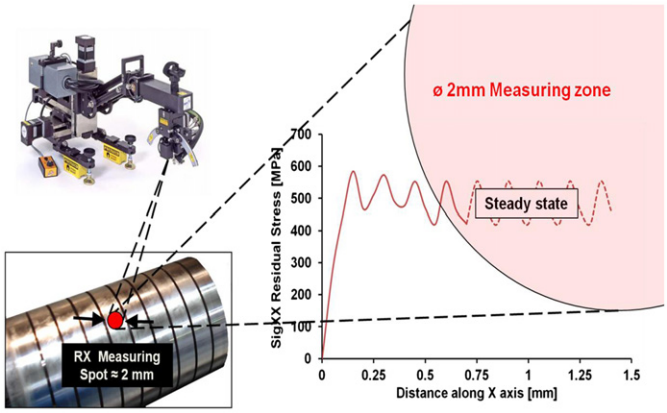

Fig. 21. Comparison of the calculated residual stress profile on the surface and the measuring spot size of the X-ray machine.

3.3.2. *Experimental results*

Fig. 20 presents the measured residual stress profiles obtained for three feeds (0.1, 0.18 and 0.3 mm rev^{-1}), V_c=150 m min^{-1} and a_p=0.6 mm. The curve shapes are similar to the calculated ones. Here again, it appears that the feed does not significantly influence the residual stress profiles in the cutting speed direction (σ_{xx}). Only the compression peak for f=0.1 mm rev^{-1} is significantly reduced. On the contrary, the feed seems to modify the external residual stress in the feed direction (σ_{yy}) essentially.

3.4. *Discussion*

Before comparing calculated and measured residual stress profiles, it is important to recall that the spot shape of the X-ray system is a disk with a diameter of 2 mm (Fig. 21) and this measurement method averages the residual stress values inside the disk. On the contrary, the calculated profiles have shown that residual stresses are not homogeneous on the surface. The periodic variation corresponds to the feed and the variation magnitude is around 150 MPa (Fig. 17). This means that it is necessary to average the calculated residual stress values in order to compare them with experimental values (Fig. 21). This also induces an important loss of data. Much finer measuring systems should be used in the future to compare experimental and numerical results at a smaller scale (peaks and valleys of residual stresses).

Fig. 22 plots measured and calculated residual stress profiles. The measured residual stress profiles are relatively close to the calculated one, except at surface. The compression peaks are located at the same depth and compressive residual stress values are very similar (except in the cutting speed direction for f=0.3 mm rev^{-1}). Concerning residual stresses at the surface, the trends corresponding to the feed variation are similar. Nevertheless, the calculated values are always higher than the measured ones. This may be explained by unstable values due to the very strong gradient in the subsurface.

4. Conclusions

This article presents a method for 3D modeling of residual stresses generated by machining operations on 15-5PH steel. The first part of the paper presents this new approach which consists in only modeling the final machined surface of the workpiece. The hybrid model does not simulate the chip formation and the material separation around the cutting edge. But it uses thermo-mechanical loadings applied onto the machined surface.

To this end, an orthogonal cutting A.L.E. model is used to extract shapes and locations of the equivalent loadings. Based on the results of a numerical cutting model, two loading zones are taken into account: below the chip formation zone (*PSZ*) and the tool/workpiece contact zone (*TSZ*). In the *PSZ*, only a heat flux is applied whereas in the *TSZ*, a normal pressure and tangential stress are added and calibrated. The A.L.E. cutting model is not considered as a predictive one for loading quantifications. Indeed, physical phenomena around the cutting edge (friction, high strain and material behavior in extreme pressure and temperature conditions) are very difficult to precisely model. So, only shape and locations are extracted and the final quantification of loadings is made using experimentations (friction and cutting tests). Globally, the quantification and the comparison of loadings highlight the dominance of the *TSZ* loadings intensities.

Then, this new method is adapted to a 3D multipass simulation and enables to model several tool passages onto the machined surface. With this method it becomes possible to estimate the number of passages leading to a steady state. The model reveals also that residual stresses are not homogenous on the external surface. The period corresponds to the feed of the cutting tool and the $\pm$150 MPa of variation around the average value are very significant. In order to compare numerical results with experimental measurements, only the average value has been considered to obtain an accurate comparison with residual stress profiles recorded with an X-ray diffraction method. For both numerical and experimental results, the affected zone is about 0.07 mm and the external layer is always in tension followed by a compression peak below the surface. Finally, the calculated and measured stress values are relatively close. So, the competition between thermal loading (prone to generate tensile residual stresses) and mechanical loading (which leads to compressive stresses) is well reproduced. The next step related to the model improvement will be the consideration of the phase change during machining. This development will make it possible to test the capacities and robustness of the model in a large range

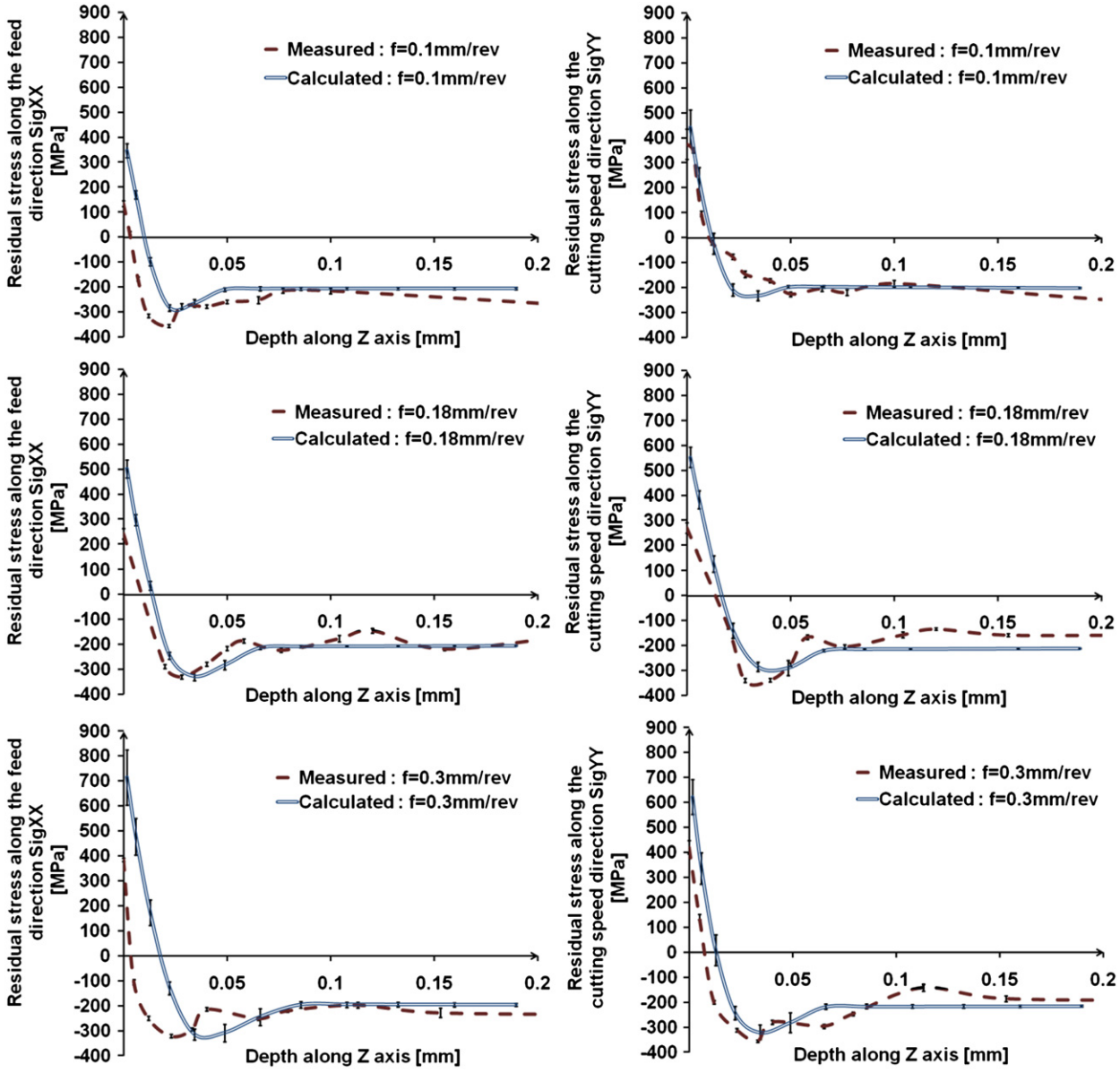

Fig. 22. Comparison of average calculated and measured residual stress profiles (V_c=150m min^{-1}, a_p=0.6 mm, f=0.1, 0.18 and 0.3 mm rev^{-1}).

of cutting parameters (change of cutting speed, worn tool, dry condition, etc.).

Acknowledgments

Authors would like to express their gratitude to the EUROCOPTER Company, the AREVA NP Company and the CETIM Company for their financial support.

References

[1] Smith S, Melkote SN, Lara-Curzio E, Watkins TR, Allard L, Riester L. Effect of surface integrity of hard turned AISI 52100 steel on fatigue performance. Mater Sci Eng A 2007;459:337–46.
[2] Bissey-Breton S, Farré J, Vignal V, Mary N. Impact des conditions d'usinage sur la zone du matériau affectée par le procédé. Méc Ind 2007;8:193–7.
[3] Davim JP, editor. Machining: fundamentals and recent advances. Springer; 2008.
[4] Jawahir IS, Brinksmeier E, M'Saoubi R, Aspinwall DK, Outeiro JC, Meyer D, Umbrello D, Jayal AD. Surface integrity in material removal processes: recent advances. CIRP Ann—Manuf Technol 2011;60:603–26.
[5] Yang X, Liu CR, Grandt AF. An experimental study on fatigue life variance, residual stress variance, and their correlation of face-turned and ground Ti 6Al–4V samples. J Manuf Sci Eng 2002;124:809–20.
[6] Liu CR, Yang X. The scatter of surface residual stresses produced by face-turning and grinding. Mach Sci Technol 2001;5:1–21.
[7] Withers PJ. Residual stress and its role in failure. Rep Prog Phys 2007;70:2211–64.
[8] Guo YB, Warren AW, Hashimoto F. The basic relationships between residual stress, white layer, and fatigue life of hard turned and ground surfaces in rolling contact. CIRP J Manuf Sci Technol 2010;2:129–34.
[9] Rech J, Hamdi H, Valette S. Workpiece Surface integrity. In: Davim JP, editor. Machining: fundamentals and recent advances. London: Springer-Verlag; 2008.
[10] Capello E. Residual stresses in turning, Part I: influence of process parameters. J Mater Process Technol 2005;160:221–8.
[11] Agha SR, Liu CR. Experimental study on the performance of superfinish hard turned surfaces in rolling contact. Wear 2000;244:52–9.
[12] M'Saoubi R, Outeiro JC, Changeux B, Lebrun JL, Morao Dias A. Residual stress analysis in orthogonal machining of standard and resulfurized AISI 316L steels. J Mater Process Technol 1999;96:225–33.
[13] Henriksen EK. Residual stresses in machined surfaces. ASME Trans 1951;73:69–76.
[14] Liu CR, Barash MM. Variables governing patterns of mechanical residual stresses in machined surface. J Eng Ind—Trans ASME 1982;104:257–64.
[15] Ulutan D, Alaca B, Lazoglu I. Analytical modelling of residual stresses in machining. J Mater Process Technol 2007;183:77–87.

[16] Ulutan D, Ozel T. Machining induced surface integrity in titanium and nickel alloys: a review. Int J Mach Tools Manuf 2010;51:250–80.
[17] Deng X, Shet C. Residual stresses and strains in orthogonal metal cutting. Int J Mach Tools Manuf 2003;43:573–87.
[18] Salio M, Berruti T, De Poli G. Prediction of residual stresses distribution after turning in turbine disks. Int J Mech Sci 2006;48:976–84.
[19] Ee KC, Dillon Jr. OW, Jawahir IS. Finite element modelling of residual stresses in machining induced by cutting a tool with finite edge radius. Int J Mech Sci 2005;47:1611–68.
[20] Liu CR, Guo YB. Ultra high speed machining of A356–T6 aluminium alloys for automotive applications. Int J Mech Sci 2000;42:1069–86.
[21] Nasr MNA, Ng EG, Elbestawi MA. Modelling the effects of tool-edge radius on residual stresses when orthogonal cutting AISI 316L. Int J Mach Tools Manuf 2007;47:401–11.
[22] Yang X, Liu CR. A new stress-based model of friction behavior in machining and its significant impact on residual stresses computed by finite element method. Int J Mech Sci 2002;44:703–23.
[23] Valiorgue F, Rech J, Hamdi H, Gilles P, Bergheau JM. A new approach for the modelling of residual stresses induced by turning of 316L. J Mater Process Technol 2007;191:270–3.
[24] Hamdi H, Zahouani H, Bergheau JM. Residual stresses computation in a grinding process. J Mater Process Technol 2004;147:277–85.
[25] Sasahara H, Obikawa T, Shirakashi T. Prediction model of surface residual stress within a machined surface by combining two orthogonal models. Int J Mach. Tools Manuf 2004;44:815–22.
[26] Attanasio A, Ceretti E, Giardini C. 3D FE modelling of superficial residual stresses in turning operations. Mach Sci Technol 2009;13:317–37.
[27] Brosse A, Hamdi H, Bergheau JM. A numerical study of phase transformation during grinding. Int J Mach Mach Mater 2008;4:148–57.
[28] Mofid M, Liangchi Z. Applied mechanics in grinding, Part 7: residual stresses induced by the full coupling of mechanical deformation, thermal deformation and phase transformation. Int J Mach Tools Manuf 1999;39:1285–98.
[29] Rech J, Kermouche G, Grzesik W, García-Rosales C, Khellouki A, García-Navas V. Characterization and modelling of the residual stresses induced by belt finishing on a AISI 52100 hardened steel. J Mater Process Technol 2008;208: 187–95.
[30] Chen X, Rowe WB, McCormack DF. Analysis of the transitional temperature for tensile residual stress in grinding. J Mater Process Technol 2000;107: 216–21.
[31] Skalli N, Turbat A, Flavenot JF. Prévision des contraintes résiduelles d'origine thermique en rectification plane. Rev Fr Méc 1991;1:69–76.
[32] Brosse A, Naisson P, Hamdi H, Bergheau JM. Temperature measurement and heat flux characterization in grinding using thermography. J Mater Process Technol 2008;201:590–5.
[33] Monaghan J, MacGinley T. Modelling the orthogonal machining process using coated carbide cutting tools. Comput Mater Sci 1999;16:275–84.
[34] Budak E, Ozlu E. Development of a thermomechanical cutting process model for machining process simulations. CIRP Ann Manuf Technol 2008;57:97–100.
[35] Habibi-Bajguirani HR. The effect of ageing upon the microstructure and mechanical properties of type 15-mai PH stainless steel. Mater Sci Eng A 2002;338:142–59.
[36] Wu T. Experiment and numerical simulation of welding induced damage of stainless steel 15-5PH. PhD dissertation. Lyon: INSA; 2007.
[37] Aghaie-Khafri M, Adhami F. Hot deformation of 15-5PH stainless steel. Mater Sci Eng A 2010;527:1052–7.
[38] Courbon C, Sajn V, Kramar D, Rech J, Kosel F, Kopac J. Investigation of machining performance in high pressure jet assisted turning of Inconel 718: a numerical model. J Mater Process Technol 2011;211:1834–51.
[39] Guillot E, Bourouga B, Garnier B, Dubar L. Estimation of thermal contact parameters at a workpiece–tool interface in a HSM process. Int J Mater Form 2008;1:1031–4.
[40] Rech J, Claudin C, D'Eramo E. Identification of a friction model—application to the context of dry cutting of an AISI 1045 annealed steel with a tin coated carbide tool. Tribol Int 2009;42:738–44.
[41] Wu T, Coret C, Combescure A. Numerical simulation of welding induced damage and residual stress of martensitic steel 15-5PH. Int J Solids Struct 2008;45:4973–89.
[42] Grolleau V. Approche de la validation expérimentale des simulations numériques de la coupe avec prise en compte des phénomènes locaux à l'arête de l'outil. PhD dissertation. Ecole Centrale de Nantes; 1996.
[43] Mabrouki T, Rigal JF. A contribution to a qualitative understanding of thermo-mechanical effects during chip formation in hard turning. J Mater Process Technol 2006;176:214–21.
[44] Bonnet C, Valiorgue F, Rech J, Claudin C, Hamdi H, Bergheau JM, Gilles P. Identification of a friction model—application to the context of dry cutting of an AISI 316L austenitic stainless steel with a TiN coated carbide tool. Int J Mach Tools Manuf 2008;48:1211–23.
[45] Johnson KL. Contact mechanics. Cambridge: Cambridge University Press; 1987.
[46] Shi G, Deng X, Shet C. A finite element study of the effect of friction in orthogonal metal cutting. Finite Elem Anal Des 2002;38:863–83.
[47] Buryta D, Sowerby R, Yellowley I. Stress distributions on the rake face during orthogonal machining. Int J Mach Tools Manuf 1994;34:721–39.
[48] Schmidt AO, Roubik JR. Distribution of heat generated in drilling. ASME Trans 1949;71:245–52.
[49] Zemzemi F, Rech J, Salem WB, Dogui A, Kapsa P. Development of a friction model for the tool–chip–workpiece interfaces during dry machining of AISI4142 steel with TiN coated carbide tools. Int J Mach Mach Mater 2007;2:361–7.
[50] Challen JM, Oxley PLB. An explanation of the different regimes of friction and wear using asperity deformation models. Wear 1979;53:229–43.
[51] Li X. Study of the jet-flow rate of cooling in machining Part 1: theoretical analysis. J Mater Process Technol 1996;62 [149–15].